# CHARACTERISATION OF PORE SIZES AND CONNECTIVITY IN 3D POROUS MEDIA

Z. JIANG, K. WU, G. COUPLES, M.I.J. VAN DIJKE, K.S. SORBIE

*Institute of Petroleum Engineering, Heriot-Watt University, Edinburgh UK*

## ABSTRACT

Fluid flow in, and the thermal, electrical, and acoustic properties of, porous media are determined by the geometry and topology of the pore system. The relationship between the detailed physics governing such processes, and the pore geometry, is not completely understood. The aim of this work is to develop an efficient and accurate method for quantifying the pore geometry and topology of porous media. The objective is to extract quantified pore descriptions from which we can build well-characterized network models for simulating two- and three-phase fluid flow. 3D reservoir rock images, which have been numerically reconstructed or taken from micro-tomography, have been investigated using our pore analysis tools (PATs). Specifically, we investigate the relationship between the coordination number and the Euler-Poincaré characteristic and propose a more efficient algorithm to compute the Euler number. However, the central purpose of this paper is to present detailed algorithms for pore extraction and quantification. Based on our quantification and mapping of the pore size distribution and connectivity, we use this information as a direct input to apply an invasion percolation simulator. The calculated pressure versus volume curve reproduces the lab-measured curve very closely, suggesting that the reconstruction process produces a reasonable representation of the medium.

## 1. INTRODUCTION

The pore structure of reservoir rocks is complex, but the geometry and topology of porous rocks must be known if we wish to *a priori* predict physical rock properties. The pore geometry ultimately affects many macroscopic phenomena associated with mechanical, acoustic and fluid flow properties. The level of detail required to model a given characteristic (e.g. permeability, acoustic impedance, etc.) may vary, but in all cases, the pore geometry must be quantified, mapped and evaluated. Indeed, it is a concern of this area of research to establish how simple a model can be made such that it can still capture the essence of the particular process in question, especially for multi-phase flow properties such as relative permeability.

Due to the complex morphology of naturally occurring pore systems, fluid flow must be modeled at the pore scale using simplified network models. One commonly used approach is to represent the pore bodies by spheres connected by bonds representing the pore throats. The most difficult task in creating such a network is identifying and specifying the coordination number and the size distributions for pore bodies and pore throats. Various approaches have been proposed to derive the network structure from an analysis of three-dimensional (3D) pore geometries (Mulder, 1996). This has also been done directly from 3-D digital images, since 3D tomography has become available (Lindquist et al, 2000, Silin and Patzek, 2003).

The aim of this work is to develop efficient and accurate algorithms for mapping the pore geometry and topology of porous media both for directly scanned images (e.g. from micro CT scans) and for simulated images, e.g. generated using pore architecture models, PAMs (Wu *et al* 2006), or other approaches. In this paper, we additionally set out to: (i) develop an approach to link quantifiable measures of porous media to an accurate mapping of the pore morphology; (ii) develop a methodology for using detailed information on pore morphology as an input to an invasion percolation simulator, and to compare its results with experimental data; and (iii) investigate quantitative methods for the characterization of pore connectivity and topology.

## 2. PORE GEOMETRY AND TOPOLOGY CHARACTERISATION

### 2.1 Introduction:

Pore geometry and topology quantification contains essentially four main procedures: pore size identification; pore volume partitioning and extraction; residuals integration; and identification of the emergent pore network. After the pores have been measured and labelled, invasion percolation (mercury injection) can be simulated using the obtained pore size and connectivity information. The principles of these processes and the corresponding algorithms are explained in detail in this paper.

The original porous medium data is represented as a 3D binary image with size $SX \times SY \times SZ$, and the value of a voxel is 0 (solid) or 1 (void). Due to the complex microstructure and irregular void space shapes within porous media, an accurate definition of a "pore" is difficult. Dullien (1992) presented the concept of "pore neck" based on the minima in the mean radius of curvature (or hydraulic radius). Further work along similar lines to determine pore space characteristics has been carried out by subsequent workers (Kwiecien 1990, Zhao *et al* 1993). Zhao *et al* (1994) pointed out that many pore necks will be missed when using this approach, while other regions can be mislabeled as necks unless the search for narrowing in the sections is performed in a sufficient number of orientations with respect to the image data set. Callaghan (1991) pointed out that other methods associated with particular geometrical models also had some serious limitations. In this work, we have adapted a widely used sphere-fitting method and combined it with a non-overlapping restriction. The general idea of this algorithm is to fit and extract each pore from the pore space in descending order of aperture radius before handling any other smaller pores. The processing steps can be summarized in the following chart.

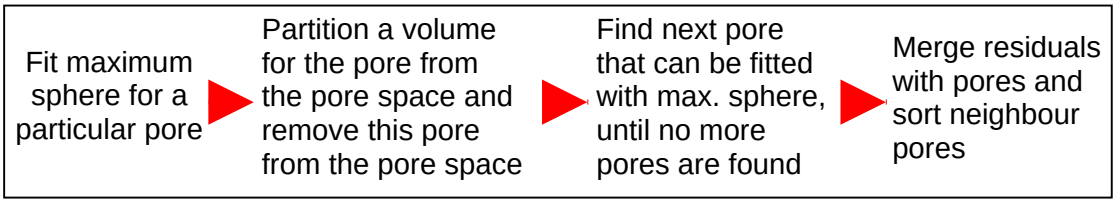


Our method to partition the pore space into sphere-equivalent components can overcome most of the shortcomings discussed above. In addition, many pore-scale geometrical and topological properties can be easily calculated based on this partitioning, such as pore size distribution, coordination number and Euler characteristic etc. The details of our method are discussed in the following sections.

## 2.2 Construction of spheres and estimation of the radius of the largest sphere:

A pore should be a protuberant 26-connected component of certain 3D shape, which implies that it should contain a certain number of voxels in its interior. The maximum inscribed sphere suitable for the target pore element (Carmeliet 2004) must describe its equivalent 3D size. To accomplish these fitting processes, template spheres are required, and these are illustrated in Fig. 1.

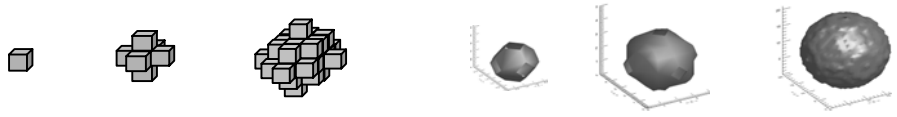

(a) (b) (c) (d) (e) (f)

**FIGURE 1:** The template discrete spheres. (a), (b) and (c): a sphere of radius 0 (single voxel), 1, 2 respectively; (d-f) corresponding to different size spheres

Then, the maximum inscribed sphere can be defined for pore space V in 3D $\subset Z^3$ and a sphere B(p,r) $\subset$ V, with centre p and radius r. B(p,r) is regarded as a maximum sphere if there exists no other sphere B(q,ŕ) (ŕ > **r )** such that B(p,r) $\subset$ B(q,ŕ) $\subset$V. Where B(p,r) is defined as

$$B(p,r) = \{q \mid dis_E(p,q) \le r, r = 1,2,\cdots\} \quad (1)$$

In our fitting algorithm, pores are extracted step by step from the corresponding 3D image of the porous medium such that the larger pores are extracted before smaller ones. An estimation of the radius of the largest inscribed sphere is important to reduce the computation time. Based on the relationship between porosity and pore size (Mulder, 1996), the largest possible pore radius can be estimated using the expression:

$$M_r = \left(\frac{3v\phi}{4\pi}\right)^{\frac{1}{3}} \quad (2)$$

where $M_r$ is the upper-limit radius of a largest sphere, $\phi$ is the porosity and ν the volume of the image. The real largest pore size will be much less than that calculated from Eq. (2). Therefore, a much smaller radius, $M_{sr} = M_r/3$, would be a reasonable value for the largest radius. In our algorithm, the sphere of radius $M_{sr}$ is first used to fit to the pore space, then successively smaller template spheres are tested.

## 2.3 Partition and extraction of pores:

Although the accurate definition of a "pore" is difficult, it usually consists of a 26/18-connected component of voxels. Most previous approaches (Lin 1982; Thovert 1993; Spanne 1994; Baldwin 1996) rely solely on morphological operations (dilation or erosion), which cannot fulfil all the requirements for detecting pore topological and geometrical properties. Therefore, a new method is investigated which combines both geometrical transformations and morphological operations. In our approach, we adopt the rule that a pore is equivalent in size to a sphere of radius r. However, there is some insensitivity to the "solid boundary noise", i.e. the irregularity in the pore geometry due to the cubic voxel structure of the pore space. Firstly, the pore must be large enough to contain an inscribed sphere with a particular size (radius), and secondly, the irregularity of the pores should be preserved as in a natural pore system.

A 26/18-connectivity porous component $X_r$ is said to be a pore of size r if:

i) there exists a sphere B(p,r-1) of radius r-1 such that B(p,r-1) $\subset X_r$

ii) the number of elements in the set of $\{p|\ p \in X_r,\ p \in B(p,r),\ p \notin B(p,r-1)\}^{\#}$ is larger than $N_{min}(r)$ where $N_{min}(r)$ is defined as follow

$$N_{\min}(r) = N_{\min}(M_{sr})[\frac{1.0-N_{\min}(1)}{M_{sr}-1}(r-1) + N_{Min}(1)] \quad (3)$$

That is, a pore of size r must completely contain a sphere of radius r-1 and should include most of the elements of a sphere of radius r. Practically, $N_{min}(M_{sr})$ and $N_{min}(1)$ are set to be 0.95, 0.65 respectively for our sandstone sample. Thus, the number of voxels in a pore of size r should be larger than the number of voxels in the current template sphere and the probability value $N_{min}(r)$ associated with the current radius r.

After a pore has been identified through the process described above, we use the cubic cutting method to remove it from the pore space to avoid overlapping with pores extracted later in the procedure (Fig. 3). Next, pores are partitioned to a corresponding cubic volume of edge length, r. Finally, the pore is combined with adjacent smaller pores under certain criteria and merged with all adjacent remaining voxels without changing pore connectivity, as explained below.

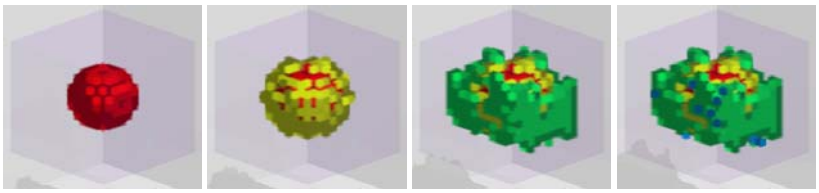

(a) (b) (c) (d)

**Fig.2:** Pore extraction processes. (a) full fitting with sphere B(p,r-1), (b) 95% fitting sphere B(p,r), (c) and (d) correspond to the subsequent cubic cutting and merging steps.

### 2.4 Merging smaller pores and remaining voxels into larger pores:

After all pores of size larger than zero have been extracted from the 3D pore space, two issues require further processing, without altering topological and geometrical features, as follows:

i) Within the pore space, there exist many remaining voxels that belong to none of the pores (radius≥1) defined above as shown in Figs. 3a to 3d;
ii) Some dead end smaller pores connect with larger pores as shown in Fig. 3e.

Therefore, we need a post-processing procedure to merge smaller pores and remaining voxels. We define criteria to partition the pore volume as explained below:

- The sets of remaining voxels, such as in Figs. 3a – 3c. The Fig. 3d blue region, which provide a connection between extracted pores, should be regarded as an individual pore to guarantee the neck property;
- The operation of merging pores and remaining voxels does not alter the topology of the original pore system, i.e. no components, no tunnels or no cavities are added or removed (as in Fig 3f red pores);
- Smaller pores that have larger adjacent pores and have no effect on the flow should be merged into the larger one, i.e. these pores are dead ends (Fig 3e red pore).

The algorithm to merge smaller pores and remaining voxels is as follows:

a) After identifying and extracting the pores from the pore space, each has a sequence number – the initial pore identification number, see Fig. 4a.

b) To cluster all remaining tiny pores (radius<1) with small numbers of voxels (< 4, as shown in Figs. 3a-3c) into various groups according to their locations and connections (Fig. 4b), referred to as the remaining components.
c) For each remaining component $P_c$, a further merging process is carried out. For $P_c$, adjacent to the initial pores, a set of all voxels of $P_c$, are tested to determine how many 26-components ($N(P_c)$) are in this set. $P_c$, is then merged into the largest adjacent pores if $N(P_c) = 1$ (see Fig. 3e), otherwise $P_c$, is regarded as a new individual pores. The merged pores are called $P_R$.
d) For each $P_R$, there are 2 cases to determine whether this pore will be combined into the largest adjacent pore: Firstly, there are less than 1/4 voxels in $P_R$ connected with solid matrix (Fig. 3e); Secondly, the number of 26-connected components in the set of voxels in its adjacent pores is <2.

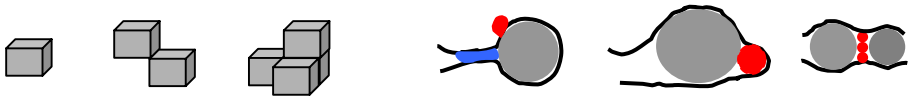


**Fig. 3:** Merging smaller pores and remaining voxels. (a), (b) and (c) are remaining voxels with radius <1. (d) small pores contribute as pore throat (blue) should be left. (e) Smaller dead end pore (red) which has only one neighbour (grey) of larger size. (f) Smaller pores (red) next to larger pore can be combined as the larger pore


**Fig. 4:** Illustration of initial pores merging with clusters of remaining voxels (different colours represent different sized pores). Left: initial pores labelled with different number; Centre: Remaining components; right: final pores after merging processing.

## 2.5 Quantification of pore connectivity – Coordination number and Euler number:

Several features of multi-phase flow depend quite critically on the pore connectivity. There is no unique quantification of this for all purposes, but the coordination number and Euler number provide measures of the local and global connectivity, respectively. The calculation methods for these quantities are explained briefly in this section.

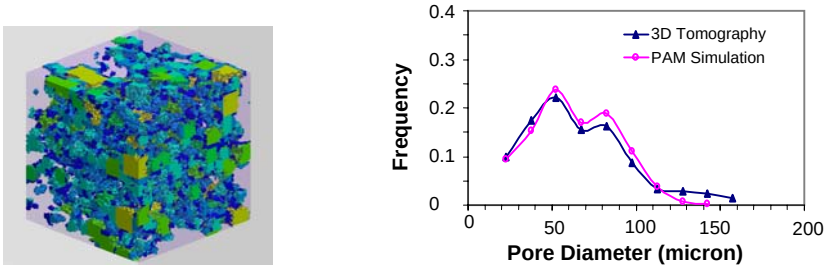


Fig 5. Illustration of various sized pores (left, different colours represent different sized pores) and pore size distribution curve (right, from 3D tomography and reconstructed sandstone)

At this point, all the pores with different radii have been extracted, and the centre of each pore has been allocated as has the centre of the corresponding interior sphere. The contact area of every neighbouring pore has also been recorded, and it is then possible to count the pore **coordination number**. 6-connectivity and 26-connectivity are commonly chosen for processing 3D images of porous media. We chose 26-connectivity in our algorithm since it considers complete connectivity. All pores in a 3D image of a porous medium can be represented as different values, in which each voxel of a pore has the same sequence number, and the coordinates of the centre of the inscribed sphere have been recorded. To find the neighbours of a pore, each voxel of the pore will be tested for its surrounding voxels using 26-connectivity. Thus, based on this data it can be determined for all neighbours of a pore if any of these belong to different pores. The coordination number distributions of sandstone 3D images from tomography and reconstruction are presented in Fig. 6a, which shows that most pores have 3 neighbours. The contact area of the pore with each neighbouring pore can be counted by deleting the voxel from the pore that has been detected as its neighbour, until every voxel in the pore connected to the neighbour has been deleted.

In general, the Euler number is defined as N-C+H, where N is the number of isolated porous objects, C is the number of tunnels, and H is the number of completely enclosed cavities. In reservoir rocks, cavities are unlikely and H should be 0. Therefore, the smaller the Euler number, the better the connectivity of porous media. There are numerous ways to calculate or estimate **Euler number** (or characteristic). Vogel (1997) proposed an approximation method. Kong et al. (1989) present a definition of Euler characteristic along with a theoretical algorithm. Saha (1995) found an approach based on classifying the direct neighbourhood, but it involved intensive computation. We propose a mew method to calculate the Euler number based on the topological number and geodesic neighbourhoods of Bertrand (Bertrand 1994). This method is fast and efficient and is discussed below.

Following Kong et al. (1989), a binary 3D image can be defined as $\mathcal{P}=(\mathcal{V}, 26,6, \mathcal{B})$, where $\mathcal{V}$ is a set of all cubic grid points, $\mathcal{B}$ is the set of all pore voxels in $\mathcal{V}$, and $\mathcal{V}$- $\mathcal{B}$ is the solid voxels. Combined with Bertrand's topological number concept and derived from Kong's algorithm, the Euler number $\chi(.)$ can be computed by the following.

$$\chi(\mathcal{V}, 26,6, \mathcal{B}) = 0 \text{ if } \mathcal{B} = \varnothing \tag{4}$$

For any other point $\mathbf{x} \in \mathcal{B}$,

$$\chi(\mathcal{V}, 26,6, \mathcal{B}) = \chi(\mathcal{V}, 26,6, \mathcal{B}-\{\mathbf{x}\}) + T_6(\mathbf{x}, \mathcal{V}-\mathcal{B}) - T_{26}(\mathbf{x}, \mathcal{B}) \tag{5}$$

where $\chi(\mathcal{V}, 26,6, \mathcal{B})$ is the Euler number; $\chi(\mathcal{V}, 26,6, \mathcal{B}-\{\mathbf{x}\})$ is the Euler number excluding this point $\mathbf{x}$; $T_6(\mathbf{x}, \mathcal{V}-\mathcal{B})$ is solid topological number of $\mathbf{x}$; $T_{26}(\mathbf{x}, \mathcal{B})$ is pore topological number of $\mathbf{x}$.

We now discuss the relationship between pore size and the global connectivity of the porous medium. In considering the effect of pore size on the connectivity, the distribution of pore connectivity against pore size can be defined as

$$\Gamma(r_0) = \chi\{ p \mid p \in \mathcal{P}_R,\ r \le r_0\}$$

where $\mathcal{P}_R$ is all pores with radius r.

Using our new algorithm, the pore connectivity distribution curve is plotted in Fig 6b which shows the Euler number vs. pore size for a sandstone sample. Obviously for the small pore sizes, the connectivity is high, as the pore size range on which $\chi$ is based comprises almost all pores. However, there is a rapid increase in the specific Euler number between pore sizes 50 - 60 μm, indicating that it is in this range (coming from the large ones downwards) that the pore space starts to be come globally connected.

## 3. SIMULATION OF MERCURY INJECTION

The pore geometry and topology data are now available to allow the simulation of mercury intrusion. Microstructural pore data can either be taken directly from 3D micro-tomography images, or it may be reconstructed using PAMs (Wu *et al* 2006). The thin section image used in the PAM reconstruction and simulated cube are given in Figs. 7a and 7b. The sample size is $200\times200\times200$ voxels with a resolution of 4.5 micron per voxel. The Lattice-Boltzmann (LB) calculated permeability of the reconstructed cube (2.2D) agrees well with the experimental value (2.5D). The mercury injection capillary pressure (MICP) curve is calculated using the usual invasion percolation algorithm; the calculated and experimental curves in Fig 7c, are in good agreement.

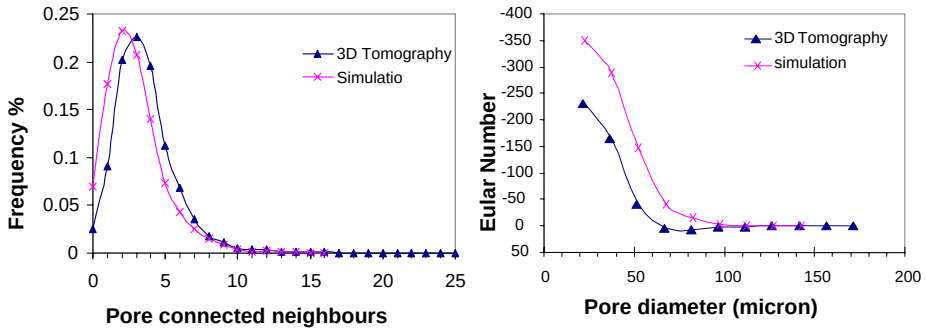


(a) (b)

FIGURE 6. (a) The coordination number distribution curve, and (b) the connectivity function (Euler number) curve from 3D tomography and reconstructed sandstones

Again, the MICP curve shows that percolation occurs at a "pore" size between 50 and 60 μm, corresponding to the rapid rise in the Euler number. Ambegokar *et al* (1971) used percolation theory to show that the "percolation radius" was associated with the average flow in the network. This radius is where, inserting bonds randomly in the network from the largest down, the network flow "switches on" or starts to conduct globally. This quantity is derived from MICP experiments and Katz and Thomson (1986; 1987) showed that an excellent correlation between the mercury breakthrough radius and the absolute permeability of various rock samples could be obtained. This early literature is applied to single and two-phase flow in O'Carroll and Sorbie (1993).

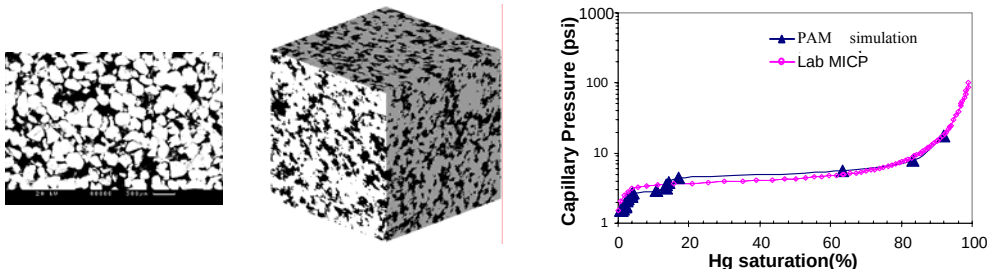


(a) (b) (c)

FIGURE **7.** (a) The sandstone thin section image, (b) a reconstructed 3D cube from the thin section image, (c) the calculated MICP curve from the invasion percolation simulator.

## 4. SUMMARY AND CONCLUSIONS

In this work, we describe the development of efficient and accurate algorithms for quantifying the pore geometry and topology of porous media. We take as our starting point, 3D rock voxel images which are either generated experimentally by micro-tomography or by a pore reconstruction methods (e.g. the PAM approach [4]). We then apply our pore analysis tools (PATs) which are a suite of algorithms which allow us to extract quantified descriptions from which we can build network models for simulating two- and three-phase fluid flow at the pore scale. Indeed, the central purpose of this paper is to present and discuss these detailed algorithms for the pore extraction and quantification. We find that the non-overlapping sphere fitting method is a simple and efficient approach for quantifying the geometry and topology of 3D images of porous media. In particular, we investigate the relationship of coordination number and Euler-Poincaré characteristic and propose an efficient algorithm to compute the Euler number. The quantification and mapping of the pore size distribution and connectivity enables us to calculate the MICP curve directly using invasion percolation. The calculated MICP curve reproduces the laboratory measured curve very closely, suggesting that the reconstruction process produces a reasonable representation of the medium. In addition, there is a clear correspondence between the rise in Euler number (between 50 and 60 μm) and the main intrusion plateau in the MICP curve where each relates to the percolation threshold, as discussed above, implying that the specific Euler number is a useful topological parameter.

There is an alternative approach for extracting the pore network from the 3D image of the pore space, known as the erosion or shrunk path method. This starts by extraction of the medial axis (pore centre/skeleton), then goes on to the identification of nodes and bonds based on its geometry and connectivity (junctions). This method will be discussed in a forthcoming paper.

The authors acknowledge funding from EPSRC under grant number EP/D002435/1.

## REFERENCES

Ambegaokar, V., Halperin, B.I., and Langer, J.S., *Phys. Rev.* B, 4 , p.2612, 1971.

Baldwin, C. A., Sederman, A. J., Mantle, M. D., Alexander, P. and Lynn F. Determination and Characterization of the Structure of a Pore Space from 3D Volume Images, *J. Colloid Interface Sci.* **181,** 79–92, 1996.

Bertrand, G., Simple points, topological numbers and geodesic neighborhoods in curbic grids, *Pattern Recognition Lett.* 15, 1003-1011, 1994.

Callaghan, P. T., ‘‘Principles of Nuclear Magnetic Resonance Microscopy.’’ Clarendon, Oxford, 1991.

Carmeliet, J. , Delerue, J.-F., Vandersteen, K. and Roels, S., Three-dimensional liquid transport in concrete cracks. *Int. J. Numer. Anal. Meth. Geomech*., 28:671–687 (DOI: 10.1002/nag.373), 2004.

Dullien, F. A. L., ‘‘Porous Media: Fluid Transport and Pore Structure.’’ Academic Press, New York, 1992.

Katz, A.J. and Thompson, A.H. , *Phys. Rev.* B, **34**, p. 8179, 1986.

Kong, T. Y. and Rosenfeld, A., Digital topology: Introduction and survey, *Comput. Vision Graphics Image Process.* 46, 357–393, 1989.

Kwiecien, M. J., Macdonald, I. F., and Dullien, F. A. L., *J. Microsc.* **159,** 343, 1990.

Lin, C., and Cohen, M. H., *J. Appl. Phys.* **53,** 4152, 1982.

Lindquist, W.B., Venkatarangan, A., Dunsmuir, J., and Wong, T. F., Pore and throat size distributions measured from synchrotron x-ray tomographic images of Fontainbleau sandstones: *J. Geophys. Res*., **105B**, 21508, 2000.

Mulder, M., Transport in porous membranes. Porous membranes for microfiltration and ultrafiltration. Casting of membranes and methods for determination of their properties, Lecture on School Membranes and Membrane Separation Techniques of Joint European Network in UMK, JEN-04720-PL-95, TorunÂ, 23±29 June 1996.

O’Carroll, C. and Sorbie, K.S., “Generalisation of the Poiseuille Law for One and Two Phase Flow in a Random Capillary Network”, *Phys. Rev.* E, **47** (No. 5), pp. 3467 – 3476, 1993.

Saha, P.K., Chaudhuri, B.B., A New Approach to Compute The Euler Characteristic, *Pattern Recognition,* **28**, No.12, pp. 1955-1963, 1995.

Silin, D, B. and Patzek, T. W., Robust determination of the pore space morphology in sedimentary rocks , *Soc. Petrol. Eng. J.,* 84296, 2003.

Spanne, P., Thovert, J. F., Jacquin, C. J., Lindquist, W. B., Jones, K. W., and Adler, P. M., *Phys. Rev. Lett.* **73**, 2001, 1994.

Thovert, J. F., Salles, J., and Adler, P. M., *J. Microsc.* **170**, 65, 1993.

Vogel, H.J., Morphological determination of pore connectivity as a function of pore size using serial sections. *Eur. J. Soil Sci*. **48**, 365–377, 1997.

Wu, K., van Dijke, M.I.J., Couples, G.D., Jiang, Z., Ma, J., Sorbie, K. S., Crawford, J., Young, I., Zhang, X., 3D Stochastic Modelling of Heterogeneous Porous Media – Applications to Reservoir Rocks, *Transport in Porous Media*, in press.

Zhao, H. Q., and Macdonald, I. F., *J. Microsc.* **172**, 157, 1993.

Zhao, H. Q., Macdonald, I. F., and Kwiecien, M. J., *J. Colloid Interface Sci.* **162**, 390, 1994.